INTERNATIONAL JOURNAL FOR NUMERICAL METHODS IN FLUIDS, VOL. 12, 463–474 (1991)

SHEDDING PATTERNS OF THE NEAR-WAKE VORTICES BEHIND A CIRCULAR CYLINDER

JONG-YOUB SA* AND KEUN-SHIK CHANG

Korea Advanced Institute of Science and Technology, PO Box 150, Cheongryang, Seoul, Republic of Korea

SUMMARY

The unsteady incompressible Navier–Stokes equations have been accurately solved for the laminar flow past a circular cylinder in the Reynolds number range 50–200. A direct elliptic solver called the SEVP is used to rapidly advance the streamfunction in time, facilitating the overall convergence to the fully periodic or quasi-steady state. A new integral-series method is developed for the far-field streamfunction condition on a finite two-dimensional computational domain. The use of fourth-order Hermitian relations for the convection terms in the conservation-form vorticity transport equation has also contributed to the good comparison of the present results with the earlier experimental data. The vortex-shedding patterns visualized by the experimentalist are numerically reproduced here in the given Reynolds number range. Discussions that may be helpful in interpreting the behaviour of the shedding frequency are presented in the main text.

KEY WORDS Circular cylinder Shedding patterns Shedding frequency modes Integral series condition

1. INTRODUCTION

The viscous flow past a circular cylinder has attracted much attention from fluid dynamicists owing to the fundamental nature of the physics and the many engineering applications. A large volume of literature associated with this particular subject attests the importance as well as complexity of the fluid flow concerned.

The Karman vortex street behind a circular cylinder has been extensively investigated in the Reynolds number range 50–200. Zdravkovich[1] found experimentally a simple mechanism responsible for the formation of the Karman vortex street in the Reynolds number range 50–120, i.e. the instability-caused sinuous oscillation of the far wake. Similar observations were also reported by Taneda[2] and Aref and Siggia.[3] Perry *et al.*,[4] on the other hand, proposed the concept of instantaneous 'alley-way' as a different mechanism for vortex street formation for a Reynolds number of order 100. They observed that it penetrated the wake cavity behind the cylinder and the vortex sheet was folded up in the way that Gerrard[5] indicated. Numerical investigation of vortex shedding has been also made by various authors such as Jordan and Fromm,[6] Martinez,[7] Lecointe and Piquet,[8] Braza *et al.*,[9] Borthwick,[10] Eaton[11] and Gresho *et al.*[12] Despite all these contributions, a theoretical account of shedding patterns has been relatively omitted from the literature.

The vortex-shedding frequency f, which alternatively implies the freestream velocity U, was measured earlier by Kovasznay.[13] An experimental correlation between the Strouhal number

* Research Associate, NASA Ames Research Center, Moffett Field, CA 94035, U.S.A.

0271–2091/91/050463–12$06.00

Received 1 September 1989
Revised 13 April 1990

($St = fd/U$, where d is the cylinder diameter) and the Reynolds number ($Re = Ud/\nu$, where ν is the kinematic viscosity) was obtained by Roshko[14] as a smooth function in the Reynolds number range $50 \leqslant Re \leqslant 150$. In contrast, Tritton[15,16] reported from his experiment two modes of shedding frequency observed for the St–Re relation: the 'low-speed mode' in the range $50 \leqslant Re \leqslant 105$ and the 'high-speed mode' in the range $80 \leqslant Re \leqslant 150$. He thought that the transition from the low-speed to the high-speed mode was due to the change of vortex-shedding mechanism near $Re = 80$. Berger[17] suggested from a careful experiment a third frequency law of vortex shedding, the so-called 'basic mode'. Another of his experiments[18] revealed that with an extremely low level of turbulence in the freestream the previous basic mode proved merely an extension of the low-speed mode, and that there existed a unified basic mode in the range $50 \leqslant Re \leqslant 160$. He thought that the mode transition was closely related to the freestream turbulence level. Berger and Wille[19] presented an early review on this controversy.

There appeared recently two additional interesting experiments related to the mode transition. Van Atta and Gharib[20] found a discontinuity of the shedding frequency caused by vortex-induced vibration, which was certainly not the kind of earlier transition. Williamson[21] observed transition of the frequency mode due to the oblique shedding from a cylinder with endplates at each end. The year-long controversy about the mode transition seems to be satisfactorily resolved by Williamson's interesting experiment. In contrast, the recent numerical study by Karniadakis and Triantafyllou[22] suggested a smooth St–Re curve.

In the present paper the vortex shedding from a circular cylinder has been simulated in the Reynolds number range $50 \leqslant Re \leqslant 200$ using an efficient and accurate numerical method developed by the authors. It was found that no mode transition appeared for the vortex-shedding frequency despite the various artificial freestream disturbances introduced in the present calculation. The vortex-shedding mechanisms claimed earlier by the experimentalists were also identified.

2. MATHEMATICAL PRELIMINARIES

A circular cylinder of radius a is transversely placed in a uniform flow of velocity U. The governing equations are first written in cylindrical polar co-ordinates (r, θ). Co-ordinate stretching $r = e^{\pi\xi}$ and $\theta = \pi\eta$ is applied to obtain the grid concentrated near the cylinder. The governing equations in conservative form are

$$\frac{\partial \zeta}{\partial t} + (\pi e^{\pi\xi})^{-2}\left[\frac{\partial}{\partial \xi}\left(\zeta \frac{\partial \psi}{\partial \eta}\right) - \frac{\partial}{\partial \eta}\left(\zeta \frac{\partial \psi}{\partial \xi}\right)\right] = \frac{2}{Re}\tilde{\nabla}^2 \zeta, \tag{1}$$

$$\tilde{\nabla}^2 \psi = -\zeta, \tag{2}$$

where

$$\tilde{\nabla}^2 \equiv (\pi e^{\pi\xi})^{-2}\left(\frac{\partial^2}{\partial \xi^2} + \frac{\partial^2}{\partial \eta^2}\right), \qquad Re = \frac{(2a)U}{\nu}.$$

The vorticity ζ and the streamfunction ψ are advanced in time by integrating equations (1) and (2) numerically. Central differencing is used for the diffusion terms. The contravariant velocity components in the convection terms of equation (1), ψ_ξ and ψ_η, are approximated by a fourth-order finite differencing called the Hermitian relation, which is discussed in the following section. Equation (1) is solved by the Euler explicit finite difference scheme and equation (2) by a direct elliptic solver explained below. The present unsteady problem requires a large number of time steps and it is mandatory that an efficient non-iterative elliptic solver be installed in the computer

code. It should be noted that many earlier time-dependent flow computations about a cylinder had to be confined to starting motion or the early transient state before a fully periodic flow was brought into the physics.

The error vector propagation (EVP) method[23-25] is a direct method applicable to any type of elliptic equations. However, as shown by McAvaney and Leslie,[26] EVP is unstable when the number of grid points is large. Madala[27] proposed a modification of this method called the SEVP (stabilized EVP) which is stable for any number of grid points and retains most of the advantages of the earlier EVP. In the SEVP method the integration region is divided into directional blocks, each of which is not taken large so that the EVP method remains stable. We have used the five-block SEVP method on 51×50 grid systems, with $\Delta\xi = 0{\cdot}02$, $\Delta\eta = 0{\cdot}04$ and $\Delta t = 0{\cdot}05$.

The four boundaries ($\overline{AB}$, $\overline{BCD}$, $\overline{DE}$ and $\overline{EFA}$) shown in Figure 1 require boundary conditions. An approximate form of the boundary data for the vorticity and the streamfunction would be on $\xi = 0$ ($\overline{EFA}$)

$$\zeta_w = -\psi_\xi|_{w+1}/(\pi e^{\pi\xi})^2 \Delta\xi,$$
$$\psi_w = 0,$$

and on $\xi = \xi_{max}$ ($\overline{BCD}$)

$$\zeta = 0 \quad \text{(at inflow boundary where } \partial\psi/\partial\eta < 0),$$
$$\partial\zeta/\partial\xi = 0 \quad \text{(at outflow boundary where } \partial\psi/\partial\eta > 0),$$
$$\psi = \psi_{far}.$$

In the above, ψ_{far} is the far-field streamfunction at the boundary of a finite computational domain evaluated by the integral series to be explained shortly. On the cut boundaries $\eta = 0$ ($\overline{AB}$) and $\eta = \eta_{max}$ ($\overline{ED}$) a continuous condition is imposed from $\theta = 2\pi$ to $\theta = 0$.

When the vortex is shed from the rear of the cylinder, periodic excursion of the forward stagnation point on the front part of the cylinder surface makes the wall streamfunction ψ_w oscillate. Jordan and Fromm[6] calculated the vortex shedding from a circular cylinder taking this migration into account. In the present problem, however, the Reynolds number is low so that the oscillation of the wall streamfunction remains extremely small. We neglected this effect to save on

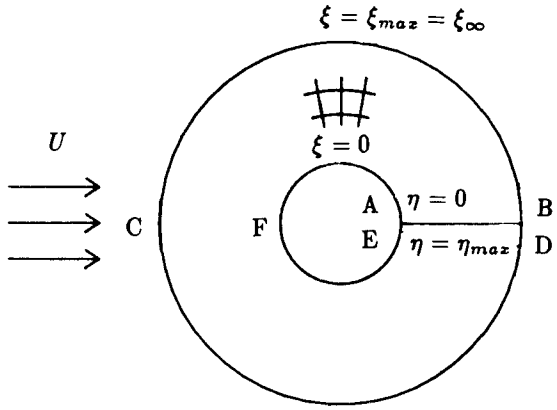

Figure 1. Flow geometry

computer time, following the practice of Borthwick.[10] A test calculation in the present work showed that the amplitude of the wall streamfunction oscillation was about 0·02 at $Re = 100$ and it hardly influenced the drag coefficient, Strouhal number, vortex-shedding patterns, etc.

The lift and the drag coefficients are defined by the equations

$$C_L = \frac{\text{lift}}{\frac{1}{2}\rho U^2(2a)} = -\int p\sin\theta\,d\theta + \frac{2}{Re}\int \zeta_w \cos\theta\,d\theta, \tag{3}$$

$$C_D = \frac{\text{drag}}{\frac{1}{2}\rho U^2(2a)} = -\int p\cos\theta\,d\theta - \frac{2}{Re}\int \zeta_w \sin\theta\,d\theta. \tag{4}$$

Integrations in the above are performed around the body surface. The wall pressure is evaluated by the finite difference

$$p_{j+1} = p_j + \frac{\Delta\eta}{Re}\left(\left.\frac{\partial\zeta}{\partial\xi}\right|_j + \left.\frac{\partial\zeta}{\partial\xi}\right|_{j+1}\right),$$

which is an approximation of the following pressure condition to second order:

$$\frac{\partial p}{\partial\eta} = \frac{2}{Re}\frac{\partial\zeta}{\partial\xi}.$$

Experimental flow visualization requires various physical tracers such as hydrogen bubbles, tufts, smoke particles and dyes. The point markers adopted in the present study as a numerical tracer were found to be a superior choice in visualizing the detailed structure of the near-wake vortices, as has also been demonstrated by Davis and co-workers[28,29] and Eaton.[11] The point markers were discharged from 14 different locations in the rear part of the circular cylinder in the present paper.

3. ON THE NUMERICAL ACCURACY

Accuracy of the numerical method cannot be overemphasized in simulating fluid flows, especially in the near wake of a cylinder where the flow is very unsteady and has large property gradients owing to the alternate vortex shedding. Care has been taken in the present paper to improve numerical accuracy in treating the two conventionally error-prone items: the non-linear convection terms and the far-boundary streamfunction condition.

The convection terms of equation (1) are in conservative form and can be discretized by central differencing as

$$\frac{\partial}{\partial\xi}(\zeta\psi_\eta) = \frac{1}{2\Delta\xi}[(\zeta\psi_\eta)_{i+1,j} - (\zeta\psi_\eta)_{i-1,j}] + O(\Delta\xi^2), \tag{5a}$$

$$\frac{\partial}{\partial\eta}(\zeta\psi_\xi) = \frac{1}{2\Delta\eta}[(\zeta\psi_\xi)_{i,j+1} - (\zeta\psi_\xi)_{i,j-1}] + O(\Delta\eta^2). \tag{5b}$$

If the central difference was repeatedly applied to the contravariant velocity components ψ_ξ and ψ_η, the intended overall second-order accuracy in space as well as the conservation property of equations (5a) and (5b) would be impaired (see the result at $Re = 200$ in Figure 4). The fourth-order Hermitian relation[30] is hereby adopted as a numerical model of the contravariant

velocities:

$$\psi_{\xi_{i-1,j}} + 4\psi_{\xi_{i,j}} + \psi_{\xi_{i+1,j}} = \frac{3}{\Delta\xi}(\psi_{i+1,j} - \psi_{i-1,j}) + O(\Delta\xi^4), \tag{6a}$$

$$\psi_{\eta_{i,j-1}} + 4\psi_{\eta_{i,j}} + \psi_{\eta_{i,j+1}} = \frac{3}{\Delta\eta}(\psi_{i,j+1} - \psi_{i,j-1}) + O(\Delta\eta^4). \tag{6b}$$

The boundary conditions for equations 6(a) and 6(b) are

$$\begin{aligned} &\psi_\xi = 0 && \text{at } \xi = 0, \\ &\psi_\xi = \partial\psi_{\text{far}}/\partial\xi && \text{at } \xi = \xi_{\max}, \\ &\psi_\eta = \text{periodic} && \text{at } \eta = 0 \text{ and } \eta = \eta_{\max}. \end{aligned}$$

Chamberlain and Liu[31] previously employed an integral-series expansion method to evaluate the vector potential at the far boundary of an unbounded domain containing two interacting vortex rings, adopting an earlier formulation of Ting.[32] Application of this series expansion method has been so far limited to the vortex-dominated flow in an open domain without any solid body within. We developed here a more generalized integral-series method for the far-field streamfunction condition ψ_{far} applicable for any number of solid bodies within an unbounded domain. It is an extension of the earlier work by Sa *et al.*[33]

We consider the Poisson equation for the streamfunction

$$\nabla^2\psi = -\zeta. \tag{7}$$

The above equation can be transformed to a Poisson integral

$$\psi(\mathbf{r}) = Uy - Vx - \frac{1}{2\pi}\left(\int\int_S \zeta_0 \ln(r')\,dS_0 + \int_{C_w} V_{b_0}\ln(r')\,dl_0\right), \tag{8}$$

where we have employed the following definitions with the integration variable $\mathbf{r}_0$:

$$\begin{aligned} \mathbf{r}' &= \mathbf{r}_0 - \mathbf{r}, \\ \zeta_0 &= \zeta(\mathbf{r}_0, t), \\ dS_0 &= dS(\mathbf{r}_0), \\ dl_0 &= dl(\mathbf{r}_0), \\ V_{b_0} &= V_b(\mathbf{r}_0). \end{aligned}$$

The last item in the above is the wall velocity component in the counterclockwise direction. The line integral in equation (8) should therefore vanish if the wall is stationary. As shown in Sa and Chang,[34] the streamfunction in equation (8) can be expanded at the far boundary as a power series of r^{-1}:

$$\psi_{\text{far}} = Uy - Vx - \frac{F_0}{2\pi}\ln(r) + \frac{1}{2\pi}\sum_{n=1}^{3}\frac{1}{n}[F_n\cos(n\theta) + G_n\sin(n\theta)]r^{-n} + O(r^{-4}), \tag{9}$$

where

$$F_0 = \iint \zeta \, dS = 0,$$

$$F_1 = \iint \zeta x \, dS, \qquad G_1 = \iint \zeta y \, dS,$$

$$F_2 = \iint \zeta (x^2 - y^2) \, dS, \qquad G_2 = \iint 2\zeta xy \, dS,$$

$$F_3 = \iint \zeta (x^3 - 3xy^2) \, dS, \qquad G_3 = \iint \zeta (3x^2 y - y^3) \, dS.$$

In the present problem under consideration, $F_n = 0$ is assumed because ψ_{far} (at $\theta = 0$ or π) is nearly zero at low Reynolds number around 100. The right-hand side of equation (9) consists of the freestream value of the streamfunction (the first two terms) plus the local correction terms made by contributions of G_n and F_n. The importance of these correction terms should not be underestimated when the computational domain has to be finite. Accuracy of the integral-series method is briefly discussed in the following section.

4. RESULTS AND DISCUSSION

The performance of the present integral-series far-boundary streamfunction condition in comparison with the conventional methods (the freestream condition, the potential flow condition

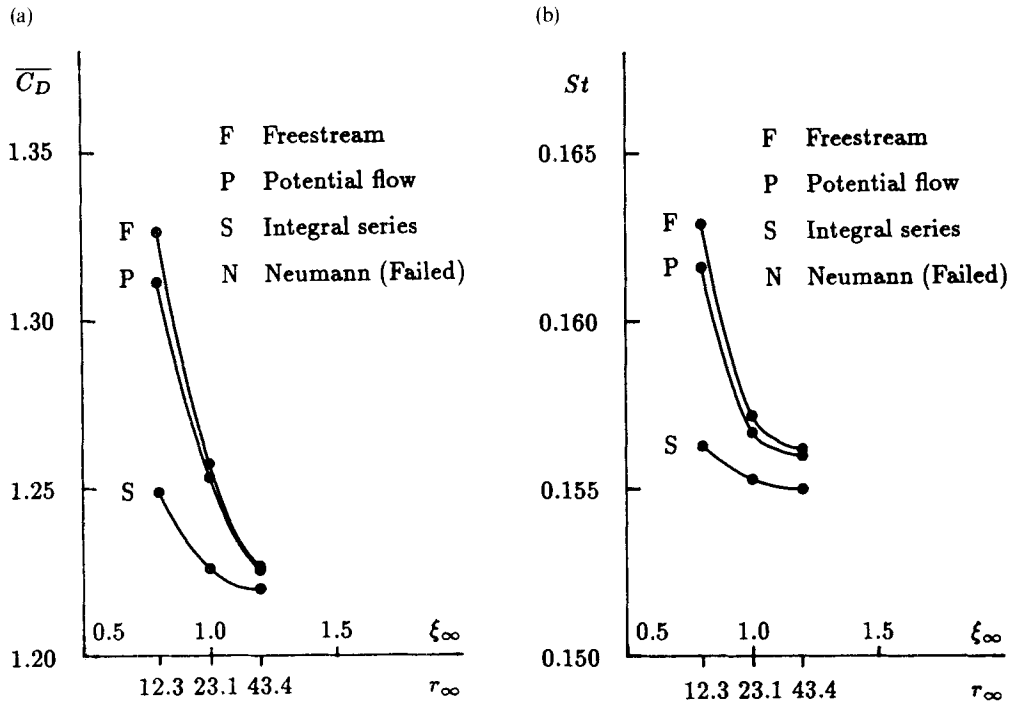

Figure 2. Comparison of numerical accuracy for different computational domains ($Re = 100$):[34] (a) drag coefficient; (b) Strouhal number

and the Neumann condition) was studied in our previous paper[34] for the flow past a circular cylinder at $Re = 100$. As shown in Figure 2, which is a reproduction, the integral-series condition gives the result nearest to the asymptotic value that would be obtained with an infinite computational domain ($r_\infty = \infty$). The freestream function condition and the potential flow condition showed a similar order of accuracy while the Neumann condition for the perturbed streamfunction failed to give any quasi-steady solution. The result of Gresho *et al.*[12] shows well that the drag coefficient and the Strouhal number have quite large values for a small computational domain of $r_\infty \approx 9$ with the freestream boundary condition when compared with other experimental and numerical results. A more detailed accuracy test can be found in Reference 34.

The present computation achieved strictly periodic vortex shedding for $Re = 100$ at about $t = 2000$. When a disturbance was introduced into the freestream in the form of $v = v_\varepsilon \sin(2\pi t/T_\varepsilon)$ during $1 \leqslant t \leqslant 1 + T_\varepsilon$, the vortex shedding reached the fully periodic state more rapidly without affecting the end result. The closed cycle of the lift–drag phase relation is demonstrated in Figure 3 for $Re = 60$ and 200, attesting the strict periodicity of the present result. The shedding frequency can be evaluated with the temporal period of the curves.

The Strouhal number, the drag coefficient and the shedding pattern calculated by the present method all agreed well with the earlier experimental results. In Table I the Strouhal numbers from the literature are listed for $Re = 100$, 150 and 200. It is concluded that the present result gives quite reasonable prediction. Figure 4 gives a comparison of the drag coefficients obtained

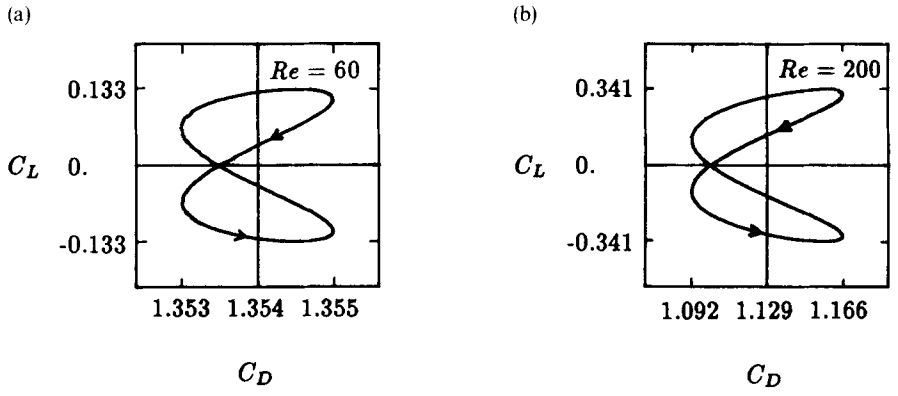

Figure 3. The lift–drag phase cycle: (a) $Re = 60$; (b) $Re = 200$

Table I. Comparison of Strouhal number

Classification	Contributor	$Re = 100$	$Re = 150$	$Re = 200$	Remarks
Numerical	Present	0·155	0·173	0·186	Strictly periodic
	Jordan and Fromm[6]	0·16			Strictly periodic
	Lecointe and Piquet[8]			0·194	Transient
	Braza *et al.*[9]	0·16		0·20	Transient
	Borthwick[10]			0·188	Nearly periodic
Experimental	Roshko[14]			0·17–0·19	
	Berger[17]		0·171		
	Nishioka and Sato[36]	0·151			
	Friehe[37]	0·145–0·165	0·165–0·185		

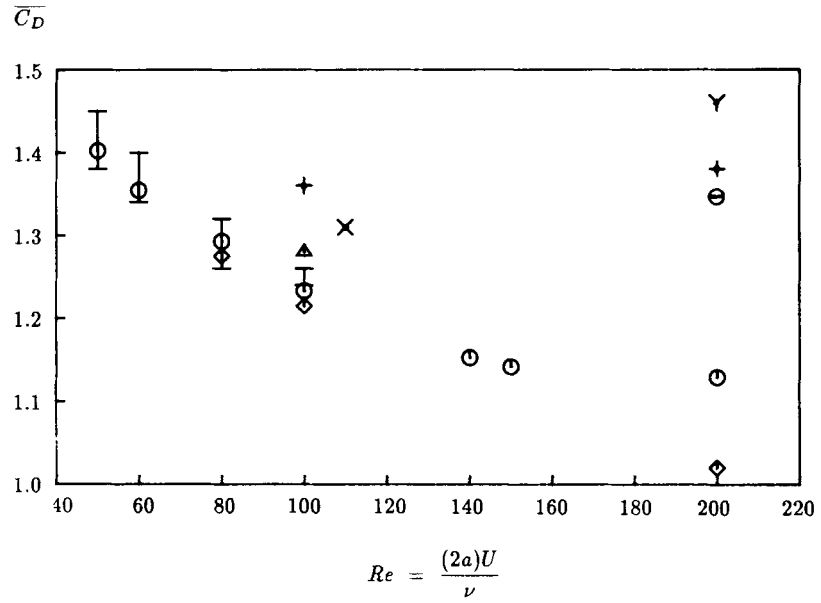

Figure 4. Time-averaged drag coefficients. Experimental: I, Tritton[15]. Numerical: Y, Lecointe and Piquet[8]; +, Braza *et al.*[9]; ×, Eaton[11]; △, Jordan and Fromm[6]; ◇, Borthwick[10]; ⊖, present result with central differencing; ⊕, present result with Hermitian relation

from various numerical methods with Tritton's experimental data. The present result agrees well with Tritton's available data for $Re \leqslant 100$. At higher Reynolds number, where experimental data are lacking, it is seen that the present result becomes most plausible among the many numerical methods as an extrapolation of Tritton's experimental data. The same figure also shows that the drag coefficient calculated by the central differencing as a test case at $Re = 200$ is drastically different from the present result of the Hermitian relation. The data points of Lecointe and Piquet[8] and Braza *et al.*[9] are even further away from the present result at $Re = 200$.

The instantaneous streamlines for vortex shedding are shown in Figure 5 for the three different Reynolds numbers. Although useful for interpretation of the shedding mechanism as Reference 4, the instantaneous streamline seems to be inadequate for visualizing the shedding pattern because the three flows are not much distinguished in Figure 5. This handicap of streamlines can be neatly solved by choosing the streaklines as an alternative tool. The numerical markers in Figure 6 presents shedding patterns remarkably similar to those experimental ones published in the literature. In the experiment, however, the smoke or dye particles are usually so congested in the immediate near wake that the detailed flow structure becomes quite ambiguous.

Tritton[15,16] suggested that near the transition Reynolds number of about 80 there was a change in the basic structure of the vortex street. Since the separated shear layer is rather weak near the Reynolds number 60, the fluid outside the wake in Figure 6(a) is hardly entrained in the wake cavity. As the Reynolds number increases, the entrainment and the consequent roll-up of the vortex sheet are prominent, as shown in Figures 6(b) and 6(c).

From Figures 5 and 6 we have noted that the vortex-shedding pattern can be better visualized by the streakline than by the streamline. The first plot for $Re = 60$ in Figure 6 does not show the roll-up of the vortex sheet, while that for $Re = 150$ indicates a strong roll-up process. Loss of numerical markers along the vortex sheet in the wake region and the increased role of both the

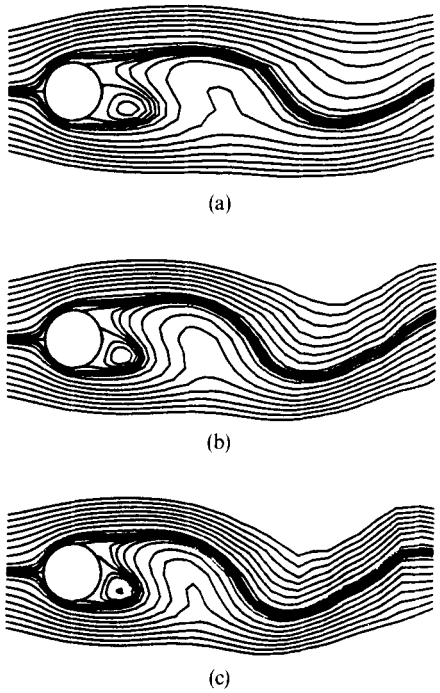

Figure 5. Instantaneous streamlines: (a) $Re = 60$; (b) $Re = 100$; (c) $Re = 150$

alley-way (introduced by Perry *et al.*[4]) and the vortex roll-up can be clearly observed in the last two plots of Figure 6. For further investigation of the change in shedding patterns we have plotted Figure 7, which shows the oscillating lift coefficient by its magnitude. The rather abrupt but not discontinuous change of slope of this curve at $Re = 80$ may be taken as evidence of such a change.

The shedding frequency calculated in the present study is compared in Figure 8 with other experimental results. The Strouhal number is evaluated by the temporal cycle of the lift–drag phase relation curves shown in Figure 3. In contrast to the smooth St–Re curve provided by Roshko[14] in the Reynolds number range 50–150, the curves by Tritton[15] exhibited two modes of shedding frequency of which the bifurcation is located near $Re = 80$. The curve for $Re \leqslant 80$ is called the low-speed mode and that for $Re \geqslant 80$ is called the high-speed mode. He conjectured that the transition from the low-speed to the high-speed mode was due to the change of the shedding mechanism. Berger[17,18] observed a third frequency law, the 'basic mode', in the Reynolds number range 120–160, with an extremely low level of freestream turbulence in his experiment. With a higher turbulence level, however, the high-speed mode was the rule of nature in the same Reynolds number range. He thought that the freestream turbulence level was closely related to Tritton's mode transition.

There are two recent experiments on shedding frequency worth mentioning. Van Atta and Gharib[20] have experimentally observed a discontinuity in the St–Re curve caused by the induced vibration. It is found that when the natural vortex-shedding frequency (for a fixed cylinder) is near the natural frequency of the cylinder vibration, the shedding frequency becomes in resonance with the latter, causing a discontinuity on the St–Re curve. However, this discontinuity has to be distinguished from the mode transition: the lock-in phenomenon of the vortex shedding merely

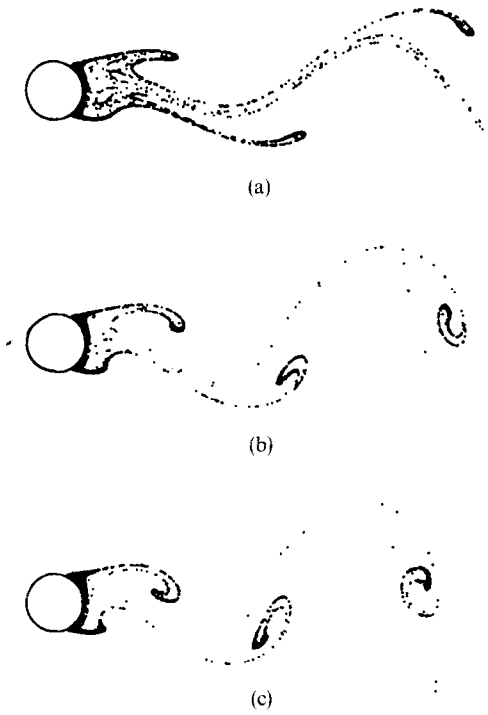

Figure 6. Streaklines: (a) $Re = 60$; (b) $Re = 100$; (c) $Re = 150$

causes a discontinuity in frequency, not the mode transition. Another interesting recent experiment by Williamson[21] showed the mode transition due to the oblique shedding from a cylinder with endplates at each end. Although the endplate condition of his cylinder is certainly different from that of Tritton and his result does not seem to explain Berger's observation concerning the effect of upstream turbulence, Williamson's result seems to be very reasonable and interesting. The influence of the endplates on the shedding frequency was also investigated by Gerich and Eckelmann.[35] Karniadakis and Triantafyllou[22] have recently studied another *St–Re* relation numerically, thus showing the continued research interest in the subject of vortex shedding from a circular cylinder.

As a different kind of application of the numerical method developed in the present paper, the authors have experimented on the influence of the freestream disturbances introduced artificially. First, a spatially uniform disturbance in the freestream speed was tried in the form of $U' = U[1 + \varepsilon \sin(2\pi f t)]$ with $f = 1, 2, 5$ and $\varepsilon = 10^{-3}, 10^{-2}, 10^{-1}$, etc. Secondly, a spatially uniform disturbance in the freestream speed having random frequency was examined. Thirdly, a random vorticity perturbation was introduced into the freestream under the constraint that the total perturbed vorticity vanishes. The mode transition has not been observed for any of these cases. It is thus believed that the mode transition cannot be possible in the absence of three-dimensional effects, as was shown by Williamson.

5. CONCLUDING REMARKS

The two mathematical traits of the present paper—the Hermitian relation used for the convection terms in the vorticity equation and the integral-series far-field streamfunction condition—have

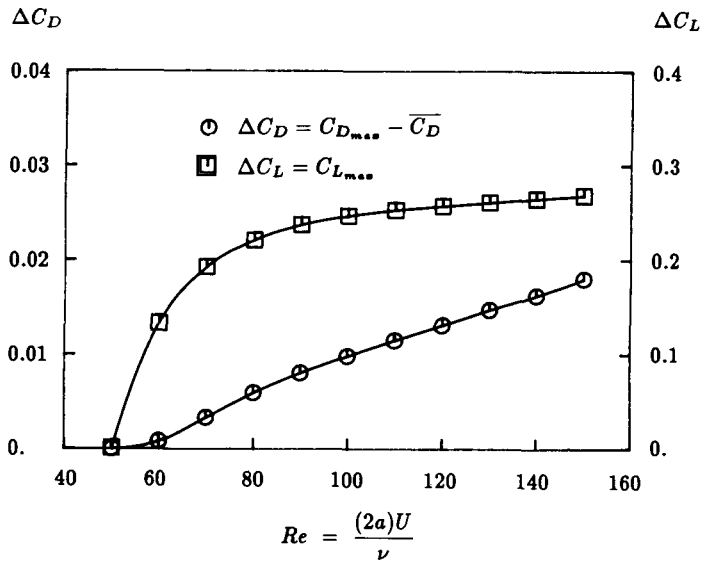

Figure 7. Oscillation amplitude of force coefficients

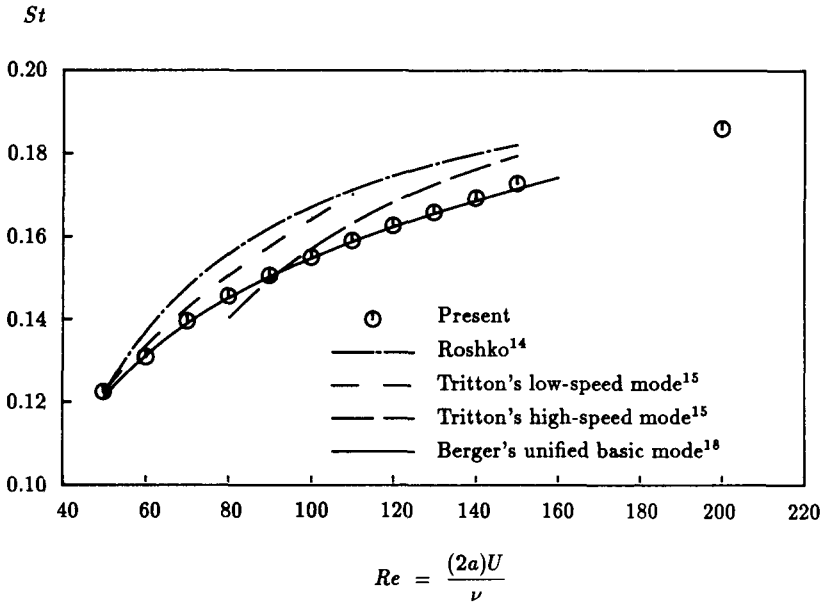

Figure 8. Vortex-shedding frequency for a circular cylinder

allowed successful numerical resolution of the delicate vortex-shedding structures in the near wake of a circular cylinder. The direct elliptic solver applied to the Poisson equation of the streamfunction also contributed to the efficient numerical solution of the otherwise lengthy and time-consuming flow computation.

As a consequence, numerical results in good agreement with the earlier measured data have been obtained in the Reynolds number range 50–200. The change in the vortex-shedding pattern

claimed by the experimentalists is supported theoretically by means of numerical streaklines and by the oscillation amplitude of the force coefficients in the limit of two-dimensional flow physics. The present study revealed that neither the change in the vortex-shedding pattern nor the two-dimensional freestream disturbances are responsible for the shedding frequency mode transition: the authors could not observe any mode transition despite a variety of significant artificial disturbances introduced into the freestream. The mode transition may thus be caused by certain three-dimensional mechanisms, e.g. the oblique shedding due to the sidewall effect as shown by Williamson.[21]

REFERENCES

1. M. M. Zdravkovich, *J. Fluid Mech.*, **37**, 491–496 (1969).
2. S. Taneda, *J. Phys. Soc. Jpn.*, **11**, 302–307 (1956).
3. H. Aref and E. D. Siggia, *J. Fluid Mech.*, **109**, 435–463 (1981).
4. A. E. Perry, M. S. Chong and T. T. Lim, *J. Fluid Mech.*, **116**, 77–90 (1982).
5. J. H. Gerrard, *Phil. Trans. R. Soc. Lond. A*, **288**, 351–382 (1978).
6. S. K. Jordan and J. E. Fromm, *Phys. Fluids*, **15**, 371–376 (1972).
7. G. Martinez, *These*, DI–INP, Toulouse, 1979.
8. Y. Lecointe and J. Piquet, *Comput. Fluids*, **12**, 255–280 (1984).
9. M. Braza, P. Chassaing and H. Ha Minh, *J. Fluid Mech.*, **165**, 79–130 (1986).
10. A. Borthwick, *Int. j. numer. methods fluids*, **6**, 275–290 (1986).
11. B. E. Eaton, *J. Fluid Mech.*, **180**, 117–145 (1987).
12. P. M. Gresho *et al.*, *Int. j. numer. methods fluids*, **4**, 619–640 (1984).
13. L. S. G. Kovasznay, *Proc. R. Soc. Lond. A*, **198**, 174–190 (1949).
14. A. Roshko, *Rep. Nat. Adv. Comm. Aero., Wash., No. 1911*, 1954.
15. D. J. Tritton, *J. Fluid Mech.*, **6**, 547–567 (1959).
16. D. J. Tritton, *J. Fluid Mech.*, **45**, 203–208 (1971).
17. E. Berger, *Z. Flugwiss.*, **12**, 41–59 (1964).
18. E. Berger, *Jahrbuch 1964 der WGLR*, 1964, p. 164.
19. E. Berger and R. Wille, *Ann. Rev. Fluid Mech.*, **4**, 313 (1972).
20. C. W. Van Atta and M. Gharib, *J. Fluid Mech.*, **174**, 113–133 (1987).
21. C. H. K. Williamson, *Phys. Fluids*, **31**, 2742–2744 (1988).
22. G. E. Karniadakis and G. S. Triantafyllou, *J. Fluid Mech.*, **199**, 441–470 (1989).
23. P. J. Roache, *Proc. Second Int. Conf. on Numerical Methods in Fluid Dynamics*, Springer, New York, 1971.
24. P. J. Roache, *Computational Fluid Dynamics*, Hermosa, Albuquerque, NM, 1975.
25. I. Hirota, T. Tokioka and M. Nishiguchi, *J. Meteorol. Soc. Jpn.*, **48**, 161 (1970).
26. B. J. McAvaney and L. M. Leslie, *J. Meteorol. Soc. Jpn.*, **50**, 136 (1972).
27. R. V. Madala, *Mon. Weather Rev.*, **106**, 1735 (1978).
28. R. W. Davis and E. F. Moore, *J. Fluid Mech.*, **116**, 475–506 (1982).
29. R. W. Davis, E. F. Moore and L. P. Purtell, *Phys. Fluids*, **27**, 46–59 (1984).
30. Ta Phuoc Loc, *J. Fluid Mech.*, **100**, 111–128 (1980).
31. J. P. Chamberlain and C. H. Liu, *AIAA Paper No. 84-0418, AIAA 22nd Aerospace Sciences Meeting*, Reno, NV, 9–12 January 1984.
32. L. Ting, *J. Fluid Mech.*, **127**, 497–506 (1983).
33. J. Y. Sa, K. S. Chang and C. H. Liu, *AIAA Paper No. 86-0561, AIAA 24th Aerospace Sciences Meeting*, Reno, NV, 6–9 January 1986.
34. J. Y. Sa and K. S. Chang, *J. Comput. Phys.*, (1990).
35. D. Gerich and H. Eckelmann, *J. Fluid Mech.*, **122**, 109–121 (1982).
36. M. Nishioka and H. Sato, *J. Fluid Mech.*, **89**, 49–60 (1978).
37. C. Friehe, *J. Fluid Mech.*, **100**, 237–241 (1980).